Dalton Transactions

PAPER

Check for updates

Synthesis and stereochemistry of chiral aza-boraspirobifluorenes with tetrahedral boron-stereogenic centers†

Yusuke Yoshigoe, [ID] * Keiichiro Hashizume and Shinichi Saito [ID] *

We have synthesized chiral aza-boraspirobifluorenes and evaluated their structural and photophysical properties. Enantiomers were separated by chiral HPLC on a semi-preparative scale, and the absolute stereochemistry was determined by comparison of experimental circular dichroism (CD) spectra and theoretical electronic CD (ECD) spectra. A kinetic analysis combined with theoretical calculations revealed that the rate-determining step of the racemization involves the cleavage of the B–N bond.

Introduction

Chiral tetrahedral boron compounds are promising optical materials[1-4] that exhibit circular dichroism (CD) or circular polarized luminescence (CPL), and that have been applied for stereoselective transformations.[5-12] A classic tetrahedral borane with four B–C bonds (BC$_4$) was reported by Torssell in 1962 (Fig. 1a).[13] Due to the high stability of the B–C bonds, BC$_4$ boranes exhibit high stereochemical stability.[14] To date, chiral tetrahedral boranes with B–N,[15-27] B–O,[28-31] B–H,[32,33] and boron–heteroatom[34-37] bonds have been synthesized and the stereochemistry of the compounds has been studied extensively. For example, Toyota has reported stable chiral tetrahedral boranes with three B–C bonds and one B–N bond (BC$_3$N), and examined the racemization process (Fig. 1b).[38] Here, the cleavage of the B–N bond is the rate-determining step. Recently, He has reported the enantioselective synthesis of BC$_3$N and BC$_2$N$_2$ boranes *via* asymmetric copper-catalyzed azide–alkyne cycloaddition (CuAAc) reactions and studied their stereochemical stability.[39]

Aza-boraspirobifluorenes, synthesized first by Ingleson *et al.* in 2015,[40] are neutral tetrahedral boranes with a BC$_3$N framework, in which the boron atom links an orthogonal π-conjugated pair of a borafluorene and an aza-borafluorene (Fig. 1c). Fukagawa *et al.* have applied these chemicals to organic fluorescent materials, *i.e.*, OLEDs.[41-43] We envisioned that chiral aza-boraspirobifluorenes, whose optical resolution and stereochemical stability have not yet been reported,[44] could be synthesized from substituted borafluorenes (Fig. 1d).

In the present study, we synthesized chiral aza-boraspirobifluorenes and evaluated their stereochemical stability. The mechanism of the racemization process is discussed based on the obtained kinetic data. The photophysical properties, including circular dichroism (CD) spectra of the homochiral compounds, were also studied.

Results and discussion

We synthesized chiral aza-boraspirobifluorene analogue **1** by two methods (Tables 1 and 2). Compound **1a** was obtained in
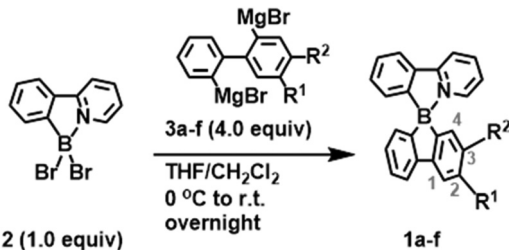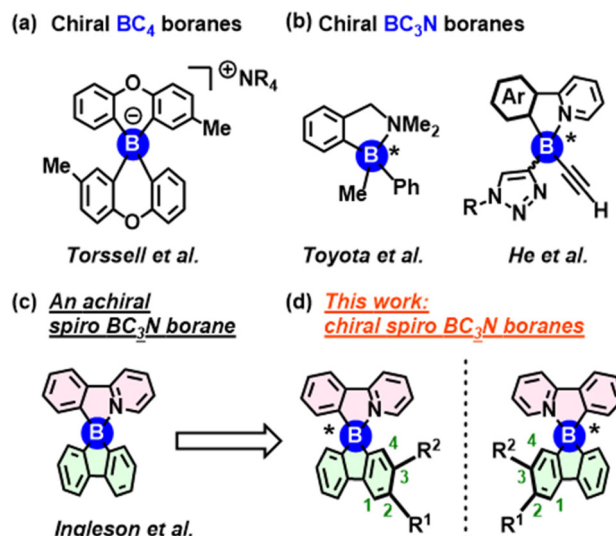

Fig. 1 (a) Chiral tetrahedral boranes with four B−C bonds (BC$_4$) reported by Torssel *et al.*; (b) chiral tetrahedral boranes with three B−C bonds and one B−N bond (BC$_3$N); (c) an achiral spiro BC$_3$N borane (aza-boraspirobifluorene); (d) this work: chiral spiro BC$_3$N boranes.
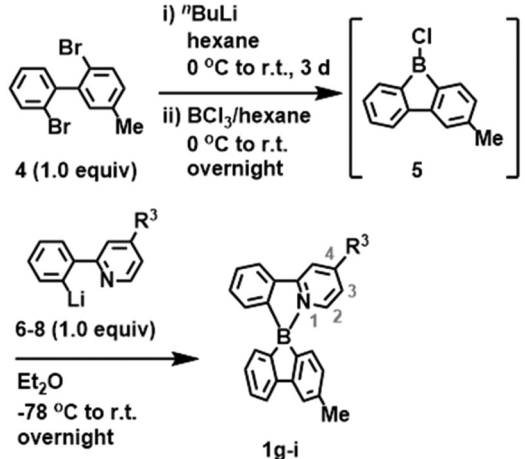
Department of Chemistry, Faculty of Science, Tokyo University of Science, Shinjuku, Tokyo 162-8601, Japan. E-mail: ssaito@rs.tus.ac.jp, yoshigoe.yusuke@rs.tus.ac.jp

Table 1 Synthesis of aza-boraspirobifluorenes **1a–f**

Entry	Reagent	R^1	R^2	1	Yield (%)
1	**3a**	H	H	**1a**	35
2	**3b**	H	H	**1b**	40
3	**3c** [a]	H	H	**1c**	20
4	**3d**	Me	H	**1d**	18
5	**3e**	OMe	H	**1e**	40
6	**3f** [a]	CF_3	H	**1f**	15

[a] The Grignard reagent was prepared by the reaction of the dibromobiphenyl derivatives, I_2-activated Mg, DIBAL-H, and LiCl.

Table 2 Synthesis of aza-boraspirobifluorenes **1g–i**

Entry	Reagent	R^3	1	Yield (%)[a]
1	**6**	Me	**1g**	24
2	**7**	OMe	**1h**	43
3	**8**	CF_3	**1i**	33

[a] Yield over two steps based on compound **4**.

35% yield by the reaction of 2-(2-(dibromoboraneyl)phenyl)pyridine (**2**)[45] with an excess (4.0 equiv.) of Grignard reagent **3a** (Table 1, entry 1). Other substituted aza-boraspirobifluorenes (**1b–e**) were obtained from the reaction of **2** with the corresponding Grignard reagents (**3b–e**) in 18–40% yield (entries 2–6).[46] The methoxy-substituted compounds **1b** and **1e** were obtained in higher yield than the other products (entries 2 and 5).

Aza-boraspirobifluorenes with substituted pyridine rings were obtained *via* a different route (Table 2). Treatment of compound **4** with [n]BuLi (2.0 equiv.), followed by the addition of a solution of BCl_3 (1.0 equiv.), furnished chloroborafluorene

5.[47,48] A solution of **5** was added to aryl lithium **6**, and **1g** was isolated in 24% yield (entry 1). The 4-methoxy derivative (**1h**) and 4-trifluoromethyl derivative (**1i**) were obtained from the corresponding aryl lithium in 43% and 33% yield, respectively (entries 2 and 3).

The solid-state structures of **1a–i** were examined by X-ray crystallography. Single crystals of **1a–i** were obtained from their solutions by slow evaporation of the solvent. The thermal-ellipsoid plot of *rac*-**1a** is shown in Fig. 2. These crystals contained (*R*)-**1a** and (*S*)-**1a** in a ratio of 1:1 within an achiral crystal system ($P2_1/c$). The tetrahedral BC_3N framework with an intramolecular B–N bond was confirmed. The torsion between the planes of the 2-phenylpyridine and biphenyl moieties was nearly orthogonal (θ = 86.4°). The B–N bond was slightly shorter (1.615(2) Å) than those of other borane–amine complexes (1.67–1.76 Å),[49,50] and close to the length of the B–C bonds (1.60–1.62 Å).[51]

Selected bond lengths and angles around the boron atom in **1a–f** are compiled in Table 3. There is no clear relationship between the substituent introduced to the aza-boraspirobifluorene and the length of the B–N bond: the bond is slightly longer in **1a** (1.615(2) Å) and slightly shorter in **1h** (1.588(7) Å), while the bond length of other compounds remained constant (1.603(3)–1.61 0(10) Å). The tetrahedral character of the dihedral angle (THC_DA)[49,52] for the spiro atoms of **1a–i** was ~50%. These values are affected by the substituents on the pyridine ring (R^3) and decrease from 62% to 29% in the order **1h** (OMe) > **1g** (Me) > **1i** (CF_3). The very small value for **1i** can be explained by the reduced Lewis basicity of the nitrogen atom upon introducing an electron-withdrawing group, which leads to an increased three-coordinated character of the boron atom. The bond lengths of B–C^1 (1.690(20) Å) and B–C^2 (1.700(10) Å) in **1i** are slightly longer than those in the other compounds.

UV/vis absorption and photoluminescence spectroscopy in CH_2Cl_2 were examined to understand the optical properties of **1a–f**. Fig. 3 shows the UV/vis absorption and fluorescence spectrum of **1d**. We observed an absorption band around 260–340 nm with a peak ($\lambda_{max, abs.}$) at 266 nm and a broad fluorescence band around 300–440 nm with two peaks ($\lambda_{max, em.}$) at 338 nm and 386 nm. Fluorescence spectra of other aza-boraspirobifluorenes composed of simple substituents emitted
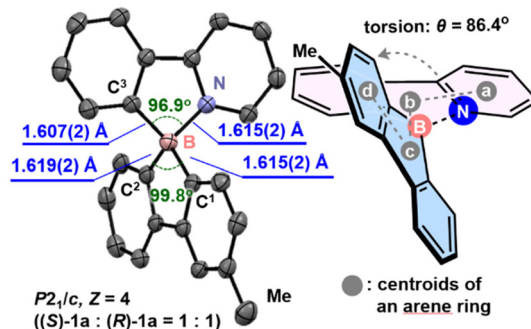

Fig. 2 Molecular structure of **1a** with thermal ellipsoids at 50% probability; hydrogen atoms are omitted for clarity.

**Table 3** Selected bond lengths and bond angles of **1a–i** [a]

	Bond length/Å				Bond angle (°)		
	B–N	B–C^1	B–C^2	B–C^3	C^{1}BC^2	C^{3}BN	THC$_{DA}$ (%) [b]
1a	1.615(2)	1.615(2)	1.619(2)	1.607(2)	99.8(1)	96.9(1)	50
1b	1.605(3)	1.608(3)	1.624(3)	1.607(3)	99.6(2)	96.7(2)	49
1c	1.603(4)	1.623(4)	1.616(3)	1.600(3)	99.6(2)	97.1(2)	49
1d	1.604(2)	1.611(3)	1.624(3)	1.609(3)	99.8(2)	97.3(2)	51
1e	1.604(2)	1.617(3)	1.622(2)	1.614(3)	99.8(1)	97.3(2)	51
1f	1.603(3)	1.618(2)	1.623(3)	1.605(2)	99.7(1)	97.4(1)	51
1g	1.610(10)	1.610(10)	1.620(10)	1.620(10)	101.1(6)	97.6(6)	54
1h	1.588(7)	1.650(10)	1.593(9)	1.610(10)	100.6(5)	98.4(5)	62
1i	1.610(2)	1.690(20)	1.700(10)	1.608(2)	91.1(8)	97.0(1)	29

[a] See Fig. 2 for assignment of the bond lengths and bond angles. [b] The tetrahedral character of the dihedral angle (THC$_{DA}$) was calculated based on six angles around the boron atom using the equation in ref. 22.
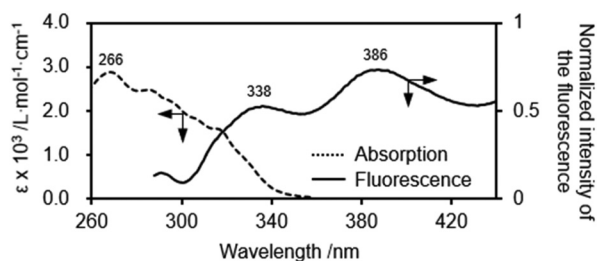
Fig. 3 Absorption (dashed) and fluorescence (solid) spectrum of **1d** (5 μM in CH$_2$Cl$_2$).

violet-blue fluorescence with $\lambda_{max, em.}$ in the range of 334–463 nm (for details, see the ESI†).

Next, we examined the separation of the enantiomers and the stereochemical stability of aza-boraspirobifluorenes **1a–i** (Fig. 4a). Using chiral HPLC, *rac*-**1d** was separated into two
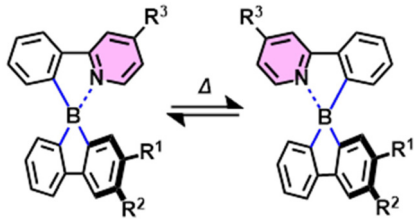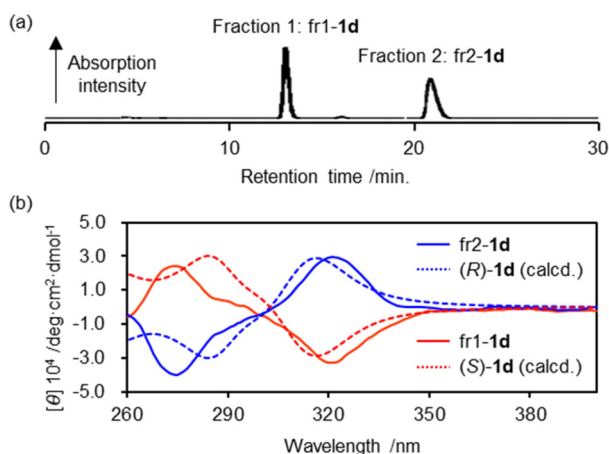

Fig. 4 (a) HPLC chart of **1d**; column: YMC CHIRAL Amylose-SA (*L* × *D*: 250 mm × 4.6 mm; particle size: 5 μm); detector: photo diode array (PDA) detector at 254 nm; eluent: *n*-hexane : CHCl$_3$: i-PrOH = 93 : 2 : 5; elution rate: 0.8 mL min^{-1}; (b) experimental CD spectra (solid) and theoretical ECD spectra (dashed) calculated at the M06-2X/6-31+G(d,p) level, whereby the structures of **1d** were optimized at the B3LYP/6-31G (d,p) level: (S)-**1d** (red) and (R)-**1d** (blue).

fractions (fr1-**1d**: ee > 99%; fr2-**1d**: ee > 99%). The CD spectra of fr1-**1d** and fr2-**1d** display mirrored Cotton effects (Fig. 4b). The spectrum for fr1-**1d** displayed a positive Cotton effect at 275 nm and a negative Cotton effect at 323 nm. The observed spectrum of fr-**1d** was in good agreement (within 10 nm) with the calculated ECD spectrum of (S)-**1d** (Fig. 4b).[53–55] Based on these results, we assigned the absolute configuration of fr1-**1d** as (S)-**1d** and that of fr2-**1d** as (R)-**1d**.
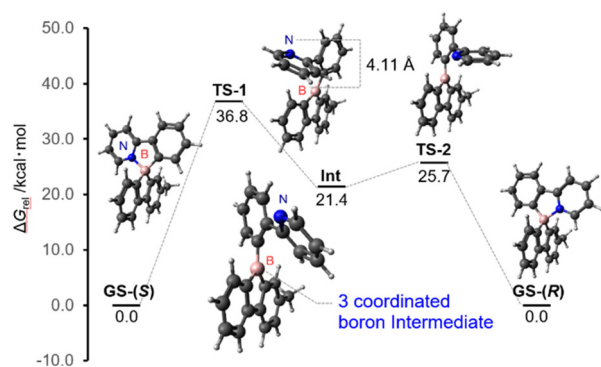
With the separated homochiral compounds in hand, we studied the racemization of **1** under various conditions. Heating a solution of (S)-**1d** in DMSO to 145 °C induced racemization.[56,57] The rate constant of racemization (k_{rac}) of (S)-**1d** at 145 °C (4.00 × 10^{-5} s^{-1}) was determined by a first-order kinetic analysis.[58–60] The kinetic parameters (145 °C: $\Delta G^{\ddagger}$ = 33.7 kcal mol^{-1}, $\Delta H^{\ddagger}$ = 26.8 kcal mol^{-1}, and $\Delta S^{\ddagger}$ = −16.6 cal K^{-1} mol^{-1}), which were determined by an Eyring-Polanyi plot at three different temperatures (135–145 °C), were higher than those of other reported BC$_3$N systems.[39,40]

The kinetic parameters for racemization of **1a–i** are summarized in Table 4. For **1a–c**, which carry a substituent at the 2-position of the borafluorene ring (R^1), $\Delta G^{\ddagger}$ increases from 32.9 kcal mol^{-1} to 34.9 kcal mol^{-1} (145 °C) in the order **1b** (R^1 = OMe) < **1a** (R^1 = Me) < **1c** (R^1 = CF$_3$). A similar trend was observed for $\Delta G^{\ddagger}$ of **1d–f**, which increases in the order **1e** (R^2 = OMe) ≃ **1d** (R^2 = Me) < **1f** (R^2 = CF$_3$). At present, we assume that the electron-withdrawing group increases the Lewis acidity of the boron atom and that the presence of a stronger B–N bond retards the racemization. For **1g–i**, which carry a substituent at the 4-positon of the aza-borafluorene ring (R^3), a clear substituent effect was observed. $\Delta G^{\ddagger}$ decreases from 33.4 to 31.0 kcal mol^{-1} in the order **1g** (R^3 = OMe) > **1h** (R^3 = Me) > **1i** (R^3 = CF$_3$). This result can be rationalized in terms of the reduced basicity of the nitrogen atom upon introducing the electron-withdrawing group. In accordance with these results, **1i**, which contains a MeO group at the 2-position of the bora-fluorene ring and a CF$_3$ group at the 4-position of the aza-bora-fluorene ring, showed the lowest activation energy ($\Delta G^{\ddagger}$ = 31.0 kcal mol^{-1}). Based on the kinetic data obtained, we concluded that the rate-determining step of the racemization involves the cleavage of the B–N bond.

Table 4 Summary of the kinetic parameters for the racemization of **1a–i**

	R^1	R^2	R^3	k_{rac} (145 °C) $10^{-5}/s^{-1}$	$\Delta G^{\ddagger}$ (145 °C)/ kcal mol^{-1}	$\Delta H^{\ddagger}$/kcal mol^{-1}
1a	Me	H	H	5.76	33.4	28.4
1b	OMe	H	H	11.3	32.9	29.6
1c	CF$_3$	H	H	0.984	34.9	33.9
1d	H	Me	H	4.00	33.7	26.8
1e	H	OMe	H	4.04	33.7	31.6
1f	H	CF$_3$	H	1.84	34.4	27.1
1g	Me	H	Me	2.70	33.4	28.4
1h	Me	H	OMe	1.77	34.4	30.7
1i	Me	H	CF$_3$	114	31.0	23.5

Fig. 5 Energy diagram for the chirality inversion from (*S*)-**1d** to (*R*)-**1d**; all calculations were carried out at the B3LYP/6-311+G(d,p)//B3LYP/6-31G(d) level.

The mechanism of racemization was further examined by theoretical calculations. The characteristic structures and the energy levels for the inversion process of (*S*)-**1d**, which were calculated at the B3LYP/6-311+G(d,p)//B3LYP/6-31G(d) level, are shown in Fig. 5. The cleavage of the B–N bond and the rotation of the B–C^3 bond can proceed *via* **Int**. The process from **GS**-(*S*) to **Int** *via* **TS-1** is favored with an activation energy of $\Delta G^{\ddagger}$ = 36.8 kcal mol^{-1}. The length of the B–N bond increases from 1.62 Å (**GS**) to 4.11 Å (**TS-1**). The rotational intermediate **Int** contains the 5-phenylborafluorene moiety, which carries a three-coordinated boron atom with no B–N interaction. Another transition state (**TS-2**) was obtained for the formation of the B–N bond.

Conclusions

We synthesized chiral aza-boraspirobifluorenes and examined their molecular structures as well as their photophysical properties. The enantiomers were separated *via* chiral HPLC. The racemization of aza-boraspirobifluorenes proceeded at elevated temperatures, and the kinetic parameters were determined to understand the mechanism of the isomerization. This study thus offers important insights into the stereochemistry of chiral tetrahedral borane compounds.

Conflicts of interest

There are no conflicts to declare.

References

1 D. Li, H. Zhang and Y. Wang, *Chem. Soc. Rev.*, 2013, **42**, 8416–8433.

2 D. Frath, J. Massue, G. Ulrich and R. Ziessel, *Angew. Chem., Int. Ed.*, 2014, **53**, 2290–2310.

3 S. K. Mellerup and S. Wang, *Chem. Soc. Rev.*, 2019, **48**, 3537–3549.

4 X. Chen, D. Tan and D.-T. Yang, *J. Mater. Chem. C*, 2022, **10**, 13499–13532.

5 D. G. Hall, *Boronic Acid*, Wiley-VCH Verlag GmbH & Co. KGaA, Weinheim, 2011.

6 M. G. Davidson, K. Wade, T. B. Marder and A. K. Hughes, *Contemporary Boron Chemistry*, Royal Society of Chemistry, Cambridge, 2000.

7 J. W. B. Fyfe and A. J. B. Watson, *Chem*, 2017, **3**, 31–55.

8 C.-Y. Wang, J. Derosa and M. R. Biscoe, *Chem. Sci.*, 2015, **6**, 5105–5113.

9 D. Leonori and V. K. Aggarwal, *Angew. Chem., Int. Ed.*, 2015, **54**, 1082–1096.

10 C. Sandford and V. K. Aggarwal, *Chem. Commun.*, 2017, **53**, 5481–5794.

11 H. Wang, C. Jing, A. Noble and V. K. Aggarwal, *Angew. Chem., Int. Ed.*, 2020, **59**, 16859–16872.

12 A. J. J. Lennox and G. C. Lloyd-Jones, *Chem. Soc. Rev.*, 2014, **43**, 421–443.

13 K. Torssell, *Acta Chem. Scand.*, 1962, **16**, 87–93.

14 D. J. Owen, D. Vanderveer and G. B. Schuster, *J. Am. Chem. Soc.*, 1998, **120**, 1705–1717.

15 L. W.-Y. Wong, A. S.-F. Au Yeung, G. S.-S. Tam, J. W.-H. Kan, H. H.-Y. Sung, F. K. Sheong, Z. Lin and I. D. Williams, *RSC Adv.*, 2018, **8**, 1451–1460.

16 L. W.-Y. Wong, J. W.-H. Kan, T.-H. Nguyen, H. H.-Y. Sung, D. Li, A. S.-F. Au-Yeung, R. Sharma, Z. Lin and I. D. Williams, *Chem. Commun.*, 2015, **51**, 15760–15763.

17 D. Uraguchi, F. Ueoka, N. Tanaka, T. Kizu, W. Takahashi and T. Ooi, *Angew. Chem., Int. Ed.*, 2020, **59**, 11456–11461.

18 J. Huskens and M. Reetz, *Eur. J. Org. Chem.*, 1999, 1775–1786.

19 D. Liu, Z. Shan, Y. Zhou, X. Wu and J. Qin, *Helv. Chim. Acta*, 2004, **87**, 2310–2317.

20 Z. He, L. Liu, Z. Zhao, S. K. Mellerup, Y. Ge, X. Wang, N. Wang and S. Wang, *Chem. – Eur. J.*, 2020, **26**, 12403–12410.

21 B. Deng, X. Wang and S. Wang, *Chem. – Eur. J.*, 2019, **25**, 14694–14700.

22 P. Novoseltseva, H. Li, X. Wang, F. Sauriol and S. Wang, *Chem. – Eur. J.*, 2020, **26**, 2276–2284.

23 M. Grandl, B. Rudolf, Y. Sun, D. F. Bechtel, A. J. Pierik and F. Pammer, *Organometallics*, 2017, **36**, 2527–2535.

24 T. A. Bartholome, J. J. Martinez, A. Kaur, D. J. D. Wilson, J. L. Dutton and C. D. Martin, *Organometallics*, 2021, **40**, 1966–1973.

25 M. Grandl, Y. Sun and F. Pammer, *Org. Chem. Front.*, 2018, **5**, 336–352.

26 F. Pammer, J. Schepper, J. Glöckler, Y. Sun and A. Orthaber, *Dalton Trans.*, 2019, **48**, 10298–10312.

27 M. Grandl, Y. Sun and F. Pammer, *Chem. – Eur. J.*, 2016, **22**, 3976–3980.

28 M. Braun, S. Schlecht, M. Engelmann, W. Frank and S. Grimme, *Eur. J. Org. Chem.*, 2008, 5221–5225.

29 P. F. Kaiser, J. M. White and C. A. Hutton, *J. Am. Chem. Soc.*, 2008, **130**, 16450–16451.

30 V. G. Jiménez, F. M. F. Santos, S. Castro-Fernández, J. M. Cuerva, P. M. P. Gois, U. Pischel and A. G. Campaña, *J. Org. Chem.*, 2018, **83**, 14057–14062.

31 S. Schlecht, W. Frank and M. Braun, *Beilstein J. Org. Chem.*, 2011, **7**, 615–621.

32 L. Charoy, A. Valleix, T. Le Gall, P. Pham Van Chuong, C. Mioskowski and L. Toupet, *Chem. Commun.*, 2000, 2275–2276.

33 C. Aupic, A. Abdou Mohamed, C. Figliola, P. Nava, B. Tuccio, G. Chouraqui, J.-L. Parrain and O. Chuzel, *Chem. Sci.*, 2019, **10**, 6524–6530.

34 L.-Y. Wang, Z.-F. Liu, K.-X. Teng, L.-Y. Niu and Q.-Z. Yang, *Chem. Commun.*, 2022, **58**, 3807–3810.

35 E. Vedejs, S. C. Fields, R. Hayashi, S. R. Hitchcock, D. R. Powell and M. R. Schrimpf, *J. Am. Chem. Soc.*, 1999, **121**, 2460–2470.

36 E. Vedejs, S. C. Fields, S. Lin and M. R. Schrimpf, *J. Org. Chem.*, 1995, **60**, 3028–3034.

37 T. Imamoto and H. Morishita, *J. Am. Chem. Soc.*, 2000, **122**, 6329–6330.

38 S. Toyota, F. Ito, N. Nitta and T. Hakamata, *Bull. Chem. Soc. Jpn.*, 2004, **77**, 2081–2088.

39 B. Zu, Y. Guo and C. He, *J. Am. Chem. Soc.*, 2021, **143**, 16302–16310.

40 D. L. Crossley, J. Cid, L. D. Curless, M. L. Turner and M. J. Ingleson, *Organometallics*, 2015, **34**(24), 5767–5774.

41 H. Fukagawa, T. Sasaki, T. Tsuzuki, Y. Nakajima, T. Takei, G. Motomura, M. Hasegawa, K. Morii and T. Shimizu, *Adv. Mater.*, 2018, **30**, 1706768.

42 H. Fukagawa, M. Hasegawa, K. Morii, K. Suzuki, T. Sasaki and T. Shimizu, *Adv. Mater.*, 2019, **31**, 1904201.

43 T. Sasaki, M. Hasegawa, K. Inagaki, H. Ito, K. Suzuki, T. Oono, K. Morii, T. Shimizu and H. Fukagawa, *Nat. Commun.*, 2021, **12**, 2706.

44 For the synthesis and chiral resolution of structurally related 9,9′-spirobifluorenes, see: C. Stobe, R. Seto, A. Schneider and A. Lützen, *Eur. J. Org. Chem.*, 2014, 6513–6518.

45 R. Wada, S. Kaga, Y. Kawai, K. Futamura, T. Murai and F. Shibahara, *Tetrahedron*, 2021, **83**, 131978.

46 Our attempts for improving the yield of **1d** were unsuccessful; for details, see the ESI.†

47 X. Mu, H. Zhang, P. Chen and G. Liu, *Chem. Sci.*, 2014, **5**, 275–280.

48 The synthesis of **5–7** was performed with reference to the synthesis of 5-chloro-5H-dibenzo[b,d]borole; for details, see: Y. Shoji, N. Tanaka, S. Muranaka, N. Shigeno, H. Sugiyama, K. Takenouchi, F. Hajjaj and T. Fukushima, *Nat. Commun.*, 2016, **7**, 12704.

49 H. Höpfl, *J. Organomet. Chem.*, 1999, **581**, 129–149.

50 S. Toyota and M. Oki, *Bull. Chem. Soc. Jpn.*, 1991, **64**, 1554–1562.

51 F. H. Allen, O. Kennard, D. G. Watson, L. Brammer, A. G. Orpen and R. Taylor, *J. Chem. Soc., Perkin Trans. 2*, 1987, S1.

52 The tetrahedral character of the dihedral angle (THCDA) can be calculated using the Höpfl equation:

$$\text{THC}_{\text{DA}} = \left[1 - \frac{\sum_{n=1-6} |109.5 - \theta_n|^\circ}{90^\circ} \right] \times 100.$$

53 H. Takekawa, K. Tanaka, E. Fukushi, K. Matsuo, T. Nehira and M. Hashimoto, *J. Nat. Prod.*, 2013, **76**, 1047–1051.

54 T. Ito and T. Nehira, *Tetrahedron Lett.*, 2014, **55**, 314–318.

55 D. J. Tantillo, *Nat. Prod. Rep.*, 2013, **30**, 1079–1086.

56 When a solution of the isolated (S)-**1d** in DMSO was kept at 25 °C without irradiation, racemization was not observed.

57 Racemization was not observed when a solution of (S)-**1d** in DMSO was irradiated with UV light (λ = 365 nm), blue LED light (λ = 460 nm), or a common domestic lamp at room temperature.

58 C. H. Bamford and C. F. H. Tipper, *Comprehensive Chemical Kinetics, vol. 1. The practice of kinetics*, Elsevier B.V., Amsterdam, 1969.

59 M. F. Boehm and J. L. Bada, *Proc. Natl. Acad. Sci. U. S. A.*, 1984, **81**, 5263–5266.

60 L. Canoira, M.-J. García-Martínez, J. F. Llamas, J. E. Ortíz and T. D. Torres, *Int. J. Chem. Kinet.*, 2003, **35**, 576–591.